

Tropical Convective Transition Statistics and Causality in the Water Vapor–Precipitation Relation

YI-HUNG KUO, J. DAVID NEELIN, AND C. ROBERTO MECHOSO

*Department of Atmospheric and Oceanic Sciences, University of California, Los Angeles,
Los Angeles, California*

(Manuscript received 15 June 2016, in final form 28 October 2016)

ABSTRACT

Previous work by various authors has pointed to the role of lower-free-tropospheric humidity in affecting the onset of deep convection in the tropics. Empirical relationships between column water vapor (CWV) and precipitation have been inferred to result from these effects. Evidence from previous work has included deep convective conditional instability calculations for entraining plumes, in which the lower-free-tropospheric environment affects the onset of deep convection due to the differential impact on buoyancy of turbulent entrainment of dry versus moist air. The relationship between deep convection and water vapor is, however, a two-way interaction because convection also moistens the free troposphere. The present study adds an additional line of evidence toward fully establishing the causality of the precipitation–water vapor relationship. Parameter perturbation experiments using the coupled Community Earth System Model (CESM) with high-time-resolution output are analyzed for a set of statistics for the transition to deep convection, coordinated with observational diagnostics for the Green Ocean Amazon (GOAmazon) campaign and tropical western Pacific Atmospheric Radiation Measurement (ARM) sites. For low values of entrainment in the deep convective scheme, these statistics are radically altered and the observed pickup of precipitation with CWV is no longer seen. In addition to helping cement the dominant direction of causality in the fast-time-scale precipitation–CWV relationship, the results point to impacts of entrainment on the climatology. Because at low entrainment convection can fire before tropospheric moistening, the climatological values of relative humidity are lower than observed. These findings can be consequential to biases in simulated climate and to projections of climate change.

1. Introduction

Previous work by various authors has identified relationships between humidity in the lower free troposphere and the onset of deep convection in the tropics, and entrainment processes have been hypothesized to be instrumental in explaining these relationships. Analysis of TOGA COARE data and subsequent modeling studies revealed that intrusions of dry air

above the planetary boundary layer into the western Pacific warm pool region tend to inhibit deep convection locally (Brown and Zhang 1997; Parsons et al. 2000; Redelsperger et al. 2002; Ridout 2002). The cloud-resolving model (CRM) and single-column model simulations confirmed the sensitivity of moist convection to lower-free-tropospheric humidity (Derbyshire et al. 2004). In the case of weak vertical wind shear, further CRM studies demonstrated that water vapor in the lower atmosphere is more critical for the onset of deep convection than sea surface temperature (Tompkins 2001). Over daily and monthly time scales, analysis of data provided by the Special Sensor Microwave Imager (SSM/I) on board orbiting satellites together with in situ measurements have revealed connections between column relative humidity (CRH) in the atmosphere and precipitation (Bretherton et al. 2004; Sobel et al. 2004). Satellite observations also showed a positive correlation between column water vapor (CWV) and precipitation anomalies during Madden–Julian oscillation (MJO;

 Denotes content that is immediately available upon publication as open access.

 Supplemental information related to this paper is available at the Journals Online website: <http://dx.doi.org/10.1175/JAS-D-16-0182.s1>.

Corresponding author e-mail: Yi-Hung Kuo, yhkuo@atmos.ucla.edu

DOI: 10.1175/JAS-D-16-0182.1

© 2017 American Meteorological Society. For information regarding reuse of this content and general copyright information, consult the [AMS Copyright Policy](#) (www.ametsoc.org/PUBSReuseLicenses).

Madden and Julian 1971) events (e.g., Waliser et al. 2009). Analysis of general circulation model (GCM) simulations found that the gross moist stability (GMS) of the atmosphere tends to lead MJO precipitation, and the GMS reduction ahead of peak MJO precipitation is due mainly to vertical advection (Benedict et al. 2014). Intercomparisons of GCM simulations have suggested that the models reproducing the most realistic MJO capture a transition from low-level moistening for light precipitation to upper-level moistening for heavy precipitation (Klingaman et al. 2015a,b). A number of studies have also examined various aspects of impacts of entrainment on model simulations: sensitivity of climatology or MJO metrics to entrainment (e.g., Bechtold et al. 2008; Zhu and Hendon 2015; Del Genio et al. 2012), the impacts of entrainment characteristics on large-scale features like double-ITCZ bias in certain GCMs (Mapes and Neale 2011; Oueslati and Bellon 2013; Hirota et al. 2014), the simulated diurnal cycle (Bechtold et al. 2004; Del Genio and Wu 2010), the coupling with boundary layer processes (Rio et al. 2009; Hourdin et al. 2013), the closure assumptions and entrainment representations in convective parameterizations (Raymond and Blyth 1986; Kuang and Bretherton 2006; Romps and Kuang 2010), and how the uncertainty of entrainment characteristics can contribute to the uncertainty in projected climate changes (Sanderson 2011; Sherwood et al. 2014).

On fast (convective) time scales, satellite observations have also revealed an empirical precipitation–CWV relationship. An outstanding feature of this relationship is the sharp increase in precipitation rate, referred to as precipitation pickup, which occurs when CWV exceeds a certain threshold value (Peters and Neelin 2006; Neelin et al. 2009). Also over the fast time scale, analyses of in situ data collected at DOE Atmospheric Radiation Measurements (ARM; Stokes and Schwartz 1994) sites over both tropical ocean (Nauru and Manus Islands in the tropical western Pacific; Mather et al. 1998) and tropical land [ARM Mobile Facility deployed at Manacapuru, Brazil, as part of the Green Ocean Amazon (GOAmazon) campaign] have revealed associations among the onset of deep convection and temporal and vertical humidity variations. These studies concluded that lower-free-tropospheric humidity affects the onset of deep convection because turbulent entrainment of dry versus moist air has different impacts on buoyancy of convective plumes (Jensen and Del Genio 2006; Holloway and Neelin 2009, 2010; Lintner et al. 2011; Schiro et al. 2016). Another conclusion was that CWV can be used as a proxy for environmental impacts on conditional instability. Estimates of entraining plume buoyancies using radiosonde

measurements in the tropical western Pacific (Holloway and Neelin 2009) and Amazon (Schiro et al. 2016), together with tropical ocean basin satellite retrievals in comparison to climate model diagnostics (Sahany et al. 2012), imply a substantial role for entrainment in explaining the observed precipitation pickup, consistent with large-eddy simulation (LES) results (Khairoutdinov and Randall 2006).

The evidence gathered from both observational and modeling approaches across various temporal and spatial scales, therefore, clearly reveals connections between free-tropospheric moistening and deep convection. Diagnostic studies and offline calculations from GCM output, however, do not alone make a full case for the causality of the observed precipitation–CWV relationship. This is because convection also acts to loft moisture (including condensate, which can subsequently reevaporate), and one must distinguish the active role of free-tropospheric moisture in affecting the onset of conditional instability from the hypothesis that CWV simply increases passively in association with convection owing to the effect of convective moistening of the column.

The present paper focuses on the dominant direction of causality in the fast-time-scale precipitation–CWV relationship and addresses the impacts of entrainment on the two-way interaction between deep convection and environmental humidity. Our methodology is based on analysis of parameter sensitivity experiments (Bernstein and Neelin 2016) in the Community Earth System Model (CESM), which is able to simulate the sharp precipitation pickup with the default setting (Sahany et al. 2012, 2014). We show that the set of statistics associated with the transition to deep convection (or “convective transition statistics”) in the CESM can be radically altered if different values of entrainment are prescribed in the deep convective scheme. In particular, the pickup of precipitation with increased CWV is no longer captured at low values of entrainment. The sensitivity of these statistics to reevaporation is also examined to quantify any contribution to the precipitation pickup that might arise from reevaporation of condensate. Furthermore, the results demonstrate that entrainment has first-order effects on the simulated climatologies of precipitation, humidity, and temperature. Because at low entrainment, convection can fire before the lower troposphere is moistened, the climatological values of relative humidity remain lower than observed in the tropics. Showing a dramatic change in convective transition statistics in absence of the entrainment pathway in a model with the two-way interaction of convection and moisture contributes an additional line of evidence for the direction of causality

in the precipitation–water vapor relationship. These findings can be consequential to a better understanding of both climatological biases and improved simulations of climate change, underscoring the importance of the examined causal pathway.

The rest of this paper is organized as follows. [Section 2](#) gives the setup of the parameter perturbation experiments, together with a brief description of the CESM and the deep convective scheme. [Section 3](#) examines composite time series of simulated precipitation, CWV, and other relevant variables for heavily precipitating events. After background on impacts of entrainment on climatology in [section 4](#), [section 5](#) presents the simulated convective transition statistics corresponding to different values of entrainment, and reevaporation rate in [section 6](#). The convective transition statistics are coordinated with observational counterparts in the study by [Schiro et al. \(2016\)](#). [Section 7](#) further explores the model composite time series, focusing on the differences due to different entrainment values and ocean–land contrast. Finally, [section 8](#) draws conclusions based on the effects of entrainment and reevaporation on the fast-time-scale statistics and discusses potential applications of our results for model diagnostics.

2. Model and data

The simulations analyzed here are integral parts of a set of parameter perturbation experiments ([Bernstein and Neelin 2016](#)) with the fully coupled Community Earth System Model, version 1.0.5 (CESM1; [Hurrell et al. 2013](#)), using CMIP5 historical greenhouse gas and aerosol forcing. The CESM simulations start from 1 January 1976, using an existing standard parameter simulation with the Community Climate System Model, version 4 (CCSM4, a subset of CESM1; [Gent et al. 2011](#)), as the initial condition. In CESM terminology this approach to starting a simulation is referred to as branch runs and aims to reduce the time required for model spinup. The atmosphere component of CESM is the Community Atmosphere Model (CAM; [Neale et al. 2010](#)) with horizontal resolution of about $1.9^\circ \times 2.5^\circ$ (latitude by longitude, 144×96 grid points) and 26 levels in the vertical. The ocean component is the Parallel Ocean Program (POP; [Smith et al. 2010](#)) with horizontal resolution of about 1° ($gx1v6$; 384×320 grid points) and 60 levels in the vertical.

The CAM deep convective scheme ([Zhang and McFarlane 1995](#), hereafter **ZM**) is based on an entraining plume calculation modified to include turbulent mixing ([Neale et al. 2008](#)) and convective momentum transports ([Richter and Rasch 2008](#)). The reevaporation of convective precipitation is also taken into account

following [Sundqvist \(1988\)](#). Here we concentrate on two sets of experiments in which the only parameter changed are the parcel fractional mean entrainment rate ($dmpdz$), which controls the entrainment of environmental air in the convective plume, and the convective precipitation evaporation rate ($zmconv_ke$, or k_e herein), which controls the reevaporation of convective precipitation, respectively. Note that $dmpdz$ is only used in the entraining plume calculations for the cloud-base mass flux closure in the **ZM** scheme. In the buoyancy computations for the rising plume at each level, a fraction (determined by $dmpdz$) of environmental air relative to updraft mass flux is assumed to be mixed into the plume, conserving dry static energy and moisture. Entrainment thus affects convection directly through the entraining plume calculations, though it may have other indirect effects. Also note that $dmpdz$ affects only deep convection (the shallow convection is handled separately). The CESM default values are $dmpdz = 1$ (units: 10^{-3} m^{-1}) and $k_e = 1$ [units: $10^{-5} (\text{kg m}^{-2} \text{ s}^{-1})^{-1/2} \text{ s}^{-1}$]. The range of $dmpdz$ explored is from 0 to 2 with default k_e , and the range of k_e explored is from 0.1 to 10 with default $dmpdz$. For $dmpdz \neq 1$ or $k_e \neq 1$, the initial state is slightly out of equilibrium because of the branch-run approach. The time scale for the simulated climate to effectively equilibrate is about 2 yr for hydrological cycle statistics including the precipitation–CWV relationship ([Bernstein and Neelin 2016](#)), although statistics affected by deep ocean circulation may not be fully equilibrated. Therefore, we can interpret that the differences obtained in the simulated convective transition statistics and climatology are due to varying entrainment or reevaporation and not to initial transients. In addition to convective precipitation given by **ZM**, the CAM also includes a calculation for large-scale precipitation, which can be produced when the environment is saturated as a result of, for example, detrainment or moisture convergence.

The CESM simulations we analyze cover the period 1976–2005 (1976–98 for auxiliary cases $dmpdz = 0.08, 0.16, 0.25$) to overlap with the data available from the Global Precipitation Climatology Project (GPCP; [Adler et al. 2003](#)), which is used as our baseline for comparison. For more details regarding the setup and coordinated parameter perturbation experiments under global warming conditions, see [Bernstein and Neelin \(2016\)](#).

Capturing the fast-time-scale convective onset requires special output from the CESM simulations. The output we analyze includes a set of relevant 2D fields at every time step for which they are computed (30 min), which can therefore be interpreted as instantaneous values as opposed to averages when model histories are written at multiple time steps. The variables selected for

analysis comprise convective and total (convective + large scale) precipitation rates (P_c and P , respectively), CWV, mass-averaged column air temperature \hat{T} , and column-integrated saturation specific humidity \hat{q}_{sat} . Here the column is defined as 1000–200 hPa. The Kahan summation algorithm (Kahan 1965) is adopted for compiling the convective transition statistics to avoid possible round-off error. For verification we use observational and reanalysis datasets, including the Remote Sensing System (RSS), version 7, microwave radiometer total column water vapor values (Hilburn and Wentz 2008), precipitation from the GPCP (version 2.2), and temperature profile from the NCEP–DOE AMIP-II Reanalysis (Reanalysis-2) dataset (Kanamitsu et al. 2002).

3. Temporal correlation between CWV and precipitation—The problem of determining causality

Previous studies analyzing observations in the maritime and continental tropics have examined composite time series centered at locally high (total) precipitation and found that CWV and precipitation are closely related, pointing to the importance of atmospheric moisture to the onset of deep convection (Holloway and Neelin 2010; Adams et al. 2013). In this section, we briefly review similar time series composites from the model to verify that causal relationships are difficult to infer from the temporal sequence alone.

Specifically, we construct composite time series of CESM output for heavy convective precipitation events at geographical locations corresponding to Manus Island (2.1°S, 146.9°E; tropical western Pacific) and the GOAmazon mobile facility near Manaus (3.1°S, 60°W; Amazon), where ARM mobile facility observational data are available (Fig. A1). Here, heavy convective precipitation events are defined as having convective precipitation rates exceeding the mean convective precipitation rate averaged over all convectively precipitating events with respect to the threshold value of 0.1 mm h^{-1} within a 96-h window at the single grid point closest to the specified location. Figure 1 shows such composites (together with those of total precipitation), centered at heavy convective precipitation events in the standard-entrainment case ($\text{dmpdz} = 1$). The qualitative features indicated by the curves in Fig. 1 are robust with respect to the value selected for the threshold defining heavy precipitation and do not change significantly if the composites are centered at locally high total precipitation (see Fig. S1). The time series of each individual heavily precipitating event may look very different from the composites shown here [e.g., see Fig. 2 in Holloway and Neelin (2010)].

At both the maritime and continental locations, the values of CWV increase (decrease) before (after) the P_c maximum, with a broad maximum surrounding the sharp precipitation maximum. This is consistent with short duration precipitation events occurring within a high-water vapor environment that tends to have longer temporal autocorrelation. Both locations are influenced by a temperature diurnal cycle, represented by \hat{q}_{sat} , which is used here as a proxy for temperature. The column relative humidity ($\text{CRH} \equiv \text{CWV}/\hat{q}_{\text{sat}}$) provides one measure of the relationship to temperature: that is, how far the column is from saturation. We note that the main impact of CWV to convection occurs via conditional instability, for which the temperature dependence is subtler than simple column saturation (Sahany et al. 2014). Vertical structure changes can reduce the usefulness of CRH relative to other measures of temperature (Neelin et al. 2009), such as lower-tropospheric layer relative humidity. In climatological analysis in section 4, we use CRH to account for large-scale temperature changes among experiments with different parameter values; CRH provides a useful measure for such equilibrated situations. At Manus Island (tropical maritime), the temporal relationship of CRH to P_c is similar to that of CWV. At the GOAmazon site (tropical continental), the diurnal cycle is stronger as seen in \hat{q}_{sat} (which is strongly influenced by boundary layer temperature). Precipitation exhibits modest diurnal cycle in these composites, while that of CWV is small. CRH has a stronger temporal structure that is not closely related with precipitation.

The model composites at Manus Island in the standard-entrainment case shown in Fig. 1 capture neither the magnitudes of precipitation rate nor the rapid CWV increase due to mesoscale processes found with observations (Fig. A1; Holloway and Neelin 2010, their Fig. 7). This is at least partially due to the model resolution. Nevertheless, the composites from the standard-entrainment case capture the relationship between environmental humidity and precipitation that has been seen from observations. The model composites at the GOAmazon site, over land, show a large amplitude in the diurnal cycle in comparison with observations (Fig. A1; Adams et al. 2013, their Fig. 2). The composites from both the model and observations show that CWV increases and decreases rather symmetrically near the precipitation maximum over both tropical maritime and continental locations examined. These features could be consistent with either the hypothesis that lower-free-tropospheric moisture has the dominant effect on convection via entrainment or the alternative hypothesis that convection simply tends to moisten the atmosphere (through detrainment or reevaporation). These,

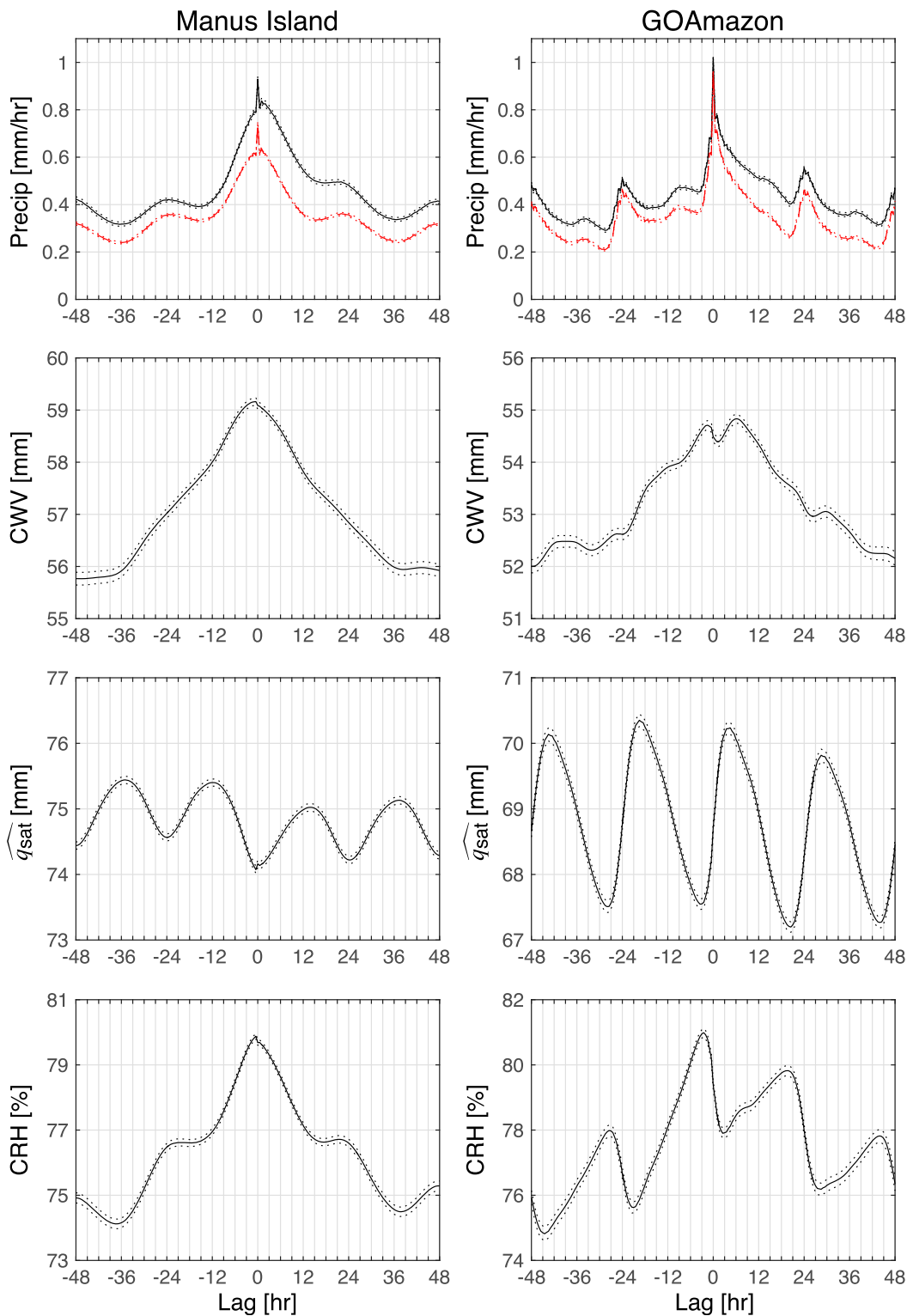


FIG. 1. Model composite time series centered at locally high convective precipitation (defined as being greater than the mean of all convectively precipitating events with respect to the threshold of 0.1 mm h^{-1}) within a 96-h window for the standard-entrainment case ($\text{dmpdz} = 1$). (top) Total (black) and convective (red) precipitation. Dotted curves in all panels represent plus or minus one standard error. The qualitative features indicated by these curves are robust with respect to the threshold defining heavy precipitation. See supplemental material for composites centered at locally high total precipitation and composites calculated using observational data.

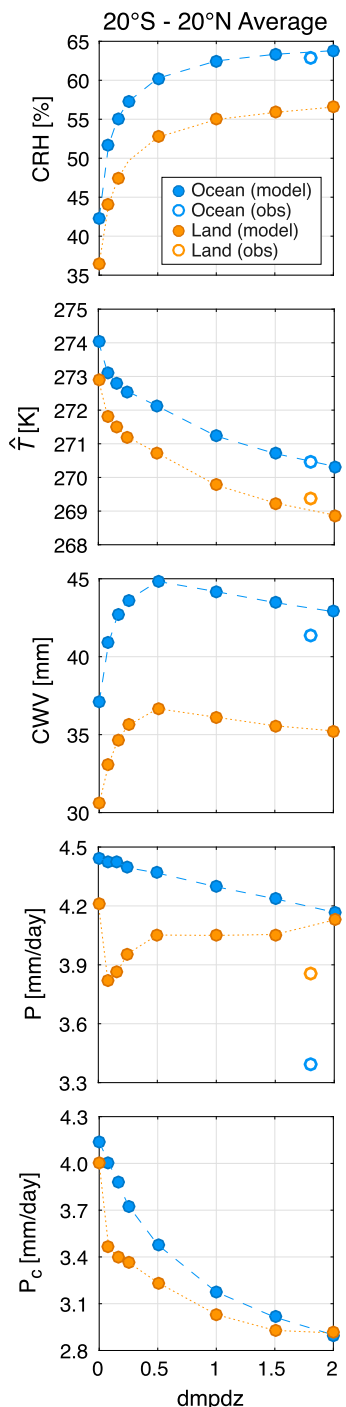


FIG. 2. Average climatological values of simulated column relative humidity (CRH), mass-averaged column air temperature \hat{T} , column-integrated water vapor (CWV), total precipitation P , and convective precipitation P_c over the tropics (20°S – 20°N) for different entrainment values $\text{dmpdz} = 0, 0.08, 0.16, 0.25, 0.5, 1, 1.5,$ and 2 . The standard errors associated with the 3-yr tropical averages are smaller than those represented by the marker size. For comparison, the corresponding values calculated using RSS CWV (over ocean), GPCP precipitation, and Reanalysis-2 temperature are also plotted at $\text{dmpdz} = 1.8$ (only for visual clarity).

however, because of the lack of asymmetry in the lead-lag relationship, are not enough to infer causality—that is, to determine whether entrainment results in the observed precipitation pickup.

In another line of evidence, radiosonde measurements from tropical ARM sites (Nauru, Manus, and GOAmazon) have shown that the moisture increase prior to deep convection tends to be in the lower free troposphere, while it tends to be in the upper troposphere after precipitation [e.g., Fig. 5 in Holloway and Neelin (2009) and Fig. 7 in Schiro et al. (2016)], consistent with composites in Sherwood and Wahrlich (1999, their Figs. 5 and 6). Such changes of vertical moisture structure associated with precipitation are potentially consistent with a causal role for lower-free-tropospheric water vapor via entrainment, with the upper-tropospheric changes due mainly to convective moistening. However, they do not alone establish causality of the observed precipitation–CWV relationship. Here we address this question by examining CESM simulations subject to different values of entrainment and reevaporation rate.

4. Climatological sensitivity to entrainment

Before turning to fast-time-scale statistics, we provide a sense of changes at the largest tropical scales in the set of parameter sensitivity experiments with different values of entrainment. As noted in the introduction, entrainment can impact the climatology simulated by GCMs. Figure 2 shows the simulated climatological values of CRH, \hat{T} , CWV, total, and convective precipitation (P and P_c , respectively), averaged over the tropics (20°S – 20°N) separately for ocean and land points as a function of entrainment parameter dmpdz . For reference, the corresponding values calculated using observational and reanalysis datasets are also plotted at $\text{dmpdz} = 1.8$. As entrainment increases, average CRH over ocean and land increases monotonically and \hat{T} decreases monotonically, with the sharpest transition for $\text{dmpdz} < 0.5$. Averaged CWV also increases drastically as dmpdz increases over both ocean and land for $\text{dmpdz} < 0.5$, after which it exhibits a slight decrease with further increase in dmpdz . This decrease at high entrainment is likely associated with decreasing \hat{T} , and CRH reasonably accounts for this temperature effect since the relationship between the boundary layer and free troposphere is fairly constant through this range. Averaged over the tropics, total precipitation is relatively insensitive to entrainment (a slow decrease with increasing entrainment over ocean, and small variations near low entrainment over land). Convective precipitation decreases modestly as dmpdz

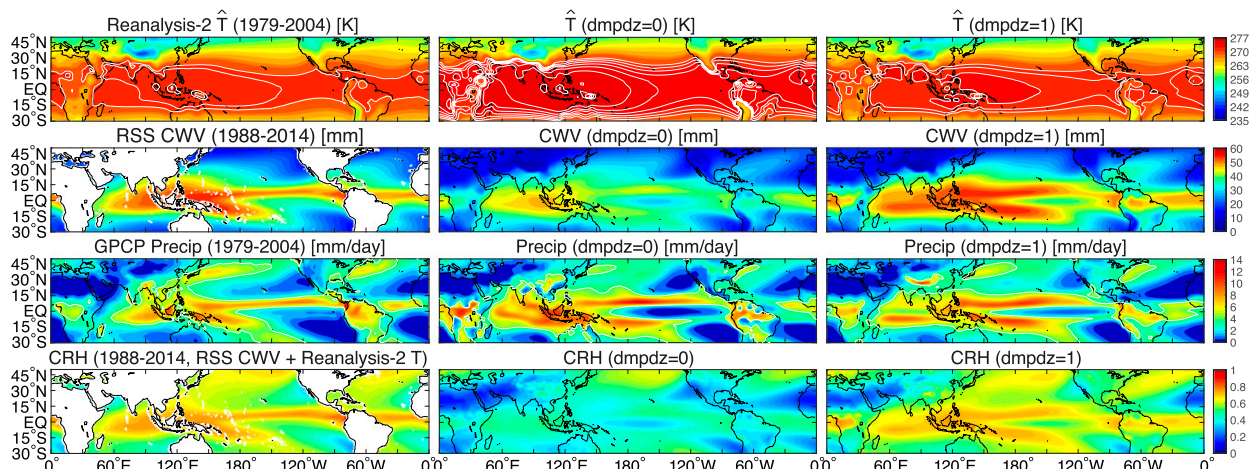


FIG. 3. Climatology of \hat{T} , CWV, P , and CRH calculated using (left) observational and reanalysis datasets, and CESM simulations for (center) no-entrainment ($dmpdz = 0$) and (right) standard-entrainment ($dmpdz = 1$) cases. White contours indicate (top) $\hat{T} \geq 270$ K with 1-K increment and (third row) the 4 mm day^{-1} contour. The climatological values for CESM simulations are calculated using the 30-min output for the period of 1979–2004, and the values for observations/reanalysis use 6-hourly and monthly data. In particular, the RSS CWV (also used for calculating CRH) is a monthly mean. The simulated CRH values calculated using the 30-min output are not very different from those calculated using monthly mean output, hence justifying the comparison here.

increases over both ocean and land, with the ratio of convective to total precipitation decreasing from 94% to 71% (ocean–land difference within 2%). This is consistent with the more restrictive conditions on conditional instability resulting in convection firing at higher CRH with increasing $dmpdz$, and with it being easier to reach saturation in the vicinity of convection associated with these higher CRH values.

The simulated precipitation in comparison with observations indicates that the simulation of the hydrologic cycle has room for improvement. Regardless of other metrics, the values of simulated CRH, \hat{T} , and CWV alone in comparison to observations/reanalysis seem to suggest a $dmpdz$ value larger than the CESM default setting, which may degrade the model performance in other aspects. For instance, Hannah and Maloney (2014) noted in the CAM5 hindcast experiments that higher entrainment values erroneously improve MJO predictive skill because of tradeoffs between vertical MSE advection and cloud–radiative feedbacks. The choice of an optimal set of parameters often involves tradeoffs among different metrics in model performance (e.g., Kim et al. 2011) and requires a systematic approach for multiobjective optimization (Langenbrunner 2015).

The dependences of simulated CRH and CWV on entrainment shown in Fig. 2 are consistent with what one would expect from entraining plume calculations, although explaining the detailed dependence of \hat{T} may require further radiation budget analysis. Over fast time scales, atmospheric moisture can be removed efficiently

through convection-induced precipitation, provided large-scale moisture divergence is negligible. When entrainment effects are included in the parameterization, convection can fire only when the environmental humidity is high enough. Thus, entrainment effects result in a moister and relatively cool atmosphere than when these effects are neglected. In contrast, without entrainment, convection occurs without preconditioning of environmental humidity; that is, the lower free troposphere does not have to moisten before conditional instability can occur. The environment thus favors a low humidity state, resulting in a moisture-depleted and relatively warm atmosphere. These CESM cases that take into account convective moistening (including reevaporation) demonstrate how the large-scale environment react to varying entrainment, serving as a background for the convective transition statistics presented in the following section.

Complementary to Fig. 2, Fig. 3 shows the climatological values of \hat{T} , CWV, total precipitation, and CRH from observational and reanalysis datasets together with those from CESM simulations for $dmpdz = 0$ and $dmpdz = 1$. Regarding the former datasets, we show \hat{T} calculated using Reanalysis-2 and precipitation from GPCP, both of which are for the 1979–2004 period. CWV is from RSS for the 1988–2014 period. The CRH is calculated using the monthly RSS CWV and Reanalysis-2 temperature field, which is for the 1988–2014 period. Although the observational datasets cover different periods and are subject to different temporal resolutions, it does not affect our discussion. Comments on

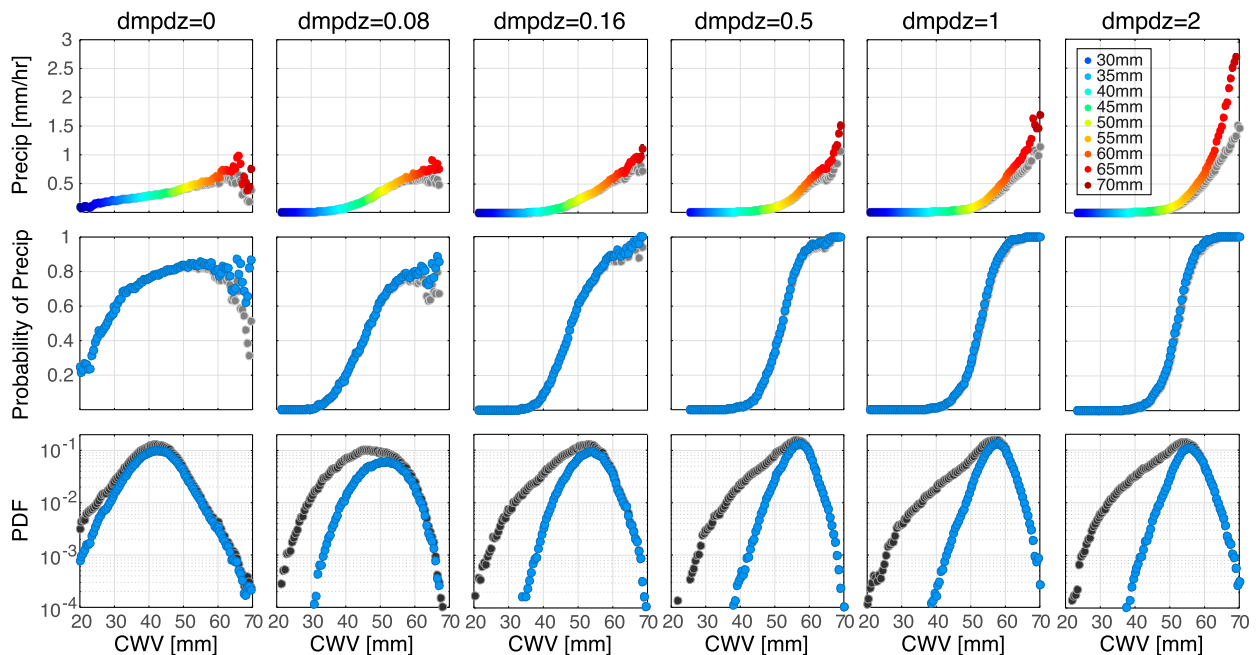


FIG. 4. The CESM-simulated convective transition statistics at Manus Island in the tropical western Pacific for various entrainment ($dmpdz$) cases. (top) The average total (color) and convective (gray) precipitation rate conditioned on CWV. (middle) The corresponding conditional probability of total (blue; $P > 0.1 \text{ mm h}^{-1}$) and convective (gray; $P_c > 0.1 \text{ mm h}^{-1}$) precipitation. (bottom) The PDF of CWV for all (dark gray) and precipitating (blue; $P > 0.1 \text{ mm h}^{-1}$) events are shown. In (top), the colors indicate the corresponding CWV value (see legend), and the standard errors associated with total precipitation rate are smaller than that represented by the marker size. Underpopulated bins ($\text{PDF} < 10^{-4}$) are trimmed and do not affect the discussion here.

biases in Reanalysis-2 CWV fields are included in the supplemental material.

Overall, Fig. 3 shows that the no-entrainment case simulates the warmest and driest atmosphere. In this case, the tropical-mean value of CWV is about 7 mm (or 13% in terms of relative difference) lower than the default case, while the corresponding CRH is lower by about 20% (or 27% in relative difference). Temperature contributes to this quantitative difference. Although not the main focus here, it is worth remarking on certain aspects of the climatological simulation. An over-extension of the South Pacific convergence zone may be noted in the tropical eastern Pacific, and the Atlantic Intertropical convection zone has excessive precipitation just south of the equator; these issues are both common in climate models (e.g., Mechoso et al. 1995; Lin 2007; Oueslati and Bellon 2015). Entrainment impacts this quantitatively, but qualitatively these issues persist across all values of entrainment examined (including in the $dmpdz = 2$ case not shown here). Large differences in precipitation occur at regional scales, but these scales can be affected by multiple parameters (Bernstein and Neelin 2016). Examination of fast-process statistics is more directly relevant to the relationships at the time scale of convection. These

statistics can provide independent measures of the convective process that can reveal differences in behavior even when it would be difficult to distinguish between effects of a parameter based on climatological metrics alone.

5. Entrainment impacts on convective transition statistics

We next turn to the simulated convective transition statistics for different values of $dmpdz$ compiled at fast time scales for two ARM sites at Manus Island in the tropical western Pacific (Fig. 4) and the GOAmazon mobile facility in the central Amazon near Manaus, Brazil (Fig. 5). For both locations we use model output sampled at the grid point including site coordinates as well as two adjacent grid points to both the east and west at both sites. The top panels in Figs. 4 and 5 show conditionally averaged precipitation rates for both total (color) and convective (gray) precipitation as a function of CWV binned at 0.5-mm intervals. The middle panels show the corresponding conditional probability of total (blue; $P > 0.1 \text{ mm h}^{-1}$) and convective (gray; $P_c > 0.1 \text{ mm h}^{-1}$) precipitation. The bottom panels show the probability distribution function (PDF) of CWV for all

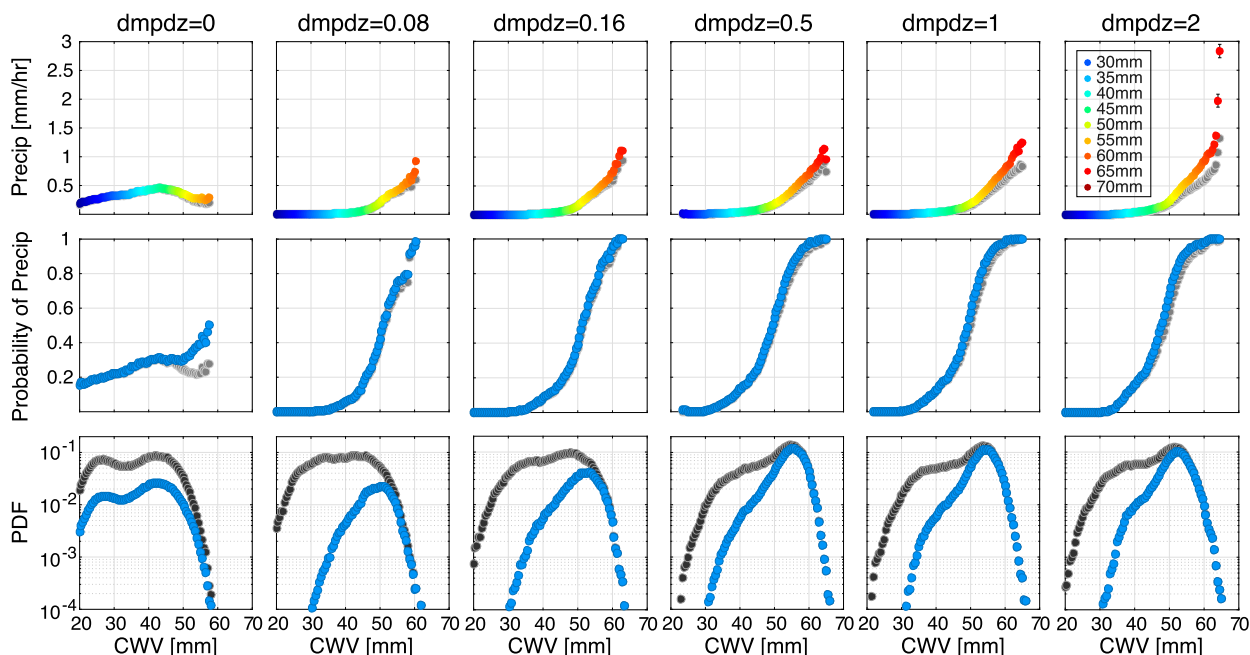


FIG. 5. As in Fig. 4, but using model output at the GOAmazon site. The standard errors associated with total precipitation rate are plotted if greater than that represented by the marker size.

(dark gray) and precipitating (blue; $P > 0.1 \text{ mm h}^{-1}$) events. Underpopulated bins ($\text{PDF} < 10^{-4}$) are trimmed and do not affect the discussion.

The convective transition statistics at tropical maritime and continental sites are qualitatively similar. For the standard case ($\text{dmpdz} = 1$), these statistics compare reasonably well to observed measures of the pickup. Observational comparisons are available from earlier studies at the ARM site at Nauru (0.5°S , 167°E ; Holloway and Neelin 2009) and satellite microwave retrievals over the tropical western Pacific (Sahany et al. 2012, 2014). A direct comparison for the GOAmazon and tropical western Pacific ARM sites may be seen in the coordinated observational paper (Schiro et al. 2016). In particular, the precipitation rate sharply increases for CWV exceeding a threshold value, known as the critical CWV. The accompanying conditional probability of precipitation picks up and the PDFs peak around this critical CWV. Quantitative discrepancies between model and observations do exist. For example, the simulated precipitation rates appear to be smaller than in observations, while the conditional probability derived from in situ data rarely reaches 80% (Schiro et al. 2016). Higher precipitation rates are noted in higher-resolution CESM runs (Sahany et al. 2012, 2014).

Drastic differences in the simulated convective transition statistics presented in Figs. 4 and 5 occur in the low entrainment range. For the no-entrainment case ($\text{dmpdz} = 0$) the precipitation pickup breaks down. At

Manus Island, conditionally averaged precipitation increases only modestly over a broad range of CWV values (Fig. 4, leftmost column). Over land at the GOAmazon site (Fig. 5, leftmost column), the precipitation actually decreases at high CWV. The probability of precipitation exhibits very different behavior than for the standard case and the observations, and the PDF for precipitating events spreads across a large range of CWV.

As entrainment increases, precipitation rate and conditional probability both evolve toward increasing functions in CWV and demonstrate clear signs of the observed pickup when subject to substantial entrainment. The precipitation rate and conditional probability curves shift toward higher CWV with increasing entrainment, consistent with the fact that larger entrainment results in a more sensitive dependence of entraining plume instability on environmental humidity. Larger entrainment also results in higher precipitation rates at the high end of CWV. The mean and mode of CWV, as being indicated by the PDF and reflected by the simulated climatology, increase as dmpdz increases from 0 to 0.5 and decrease slightly after that. This shift in climatology in response to varying entrainment matches that we see in Fig. 2. At high entrainment ($\text{dmpdz} = 1.5$ and 2), an even sharper increase of large-scale precipitation with reduced convective precipitation at very high CWV is noticed over some regions (e.g., the whole tropical western/eastern Pacific basin; not shown),

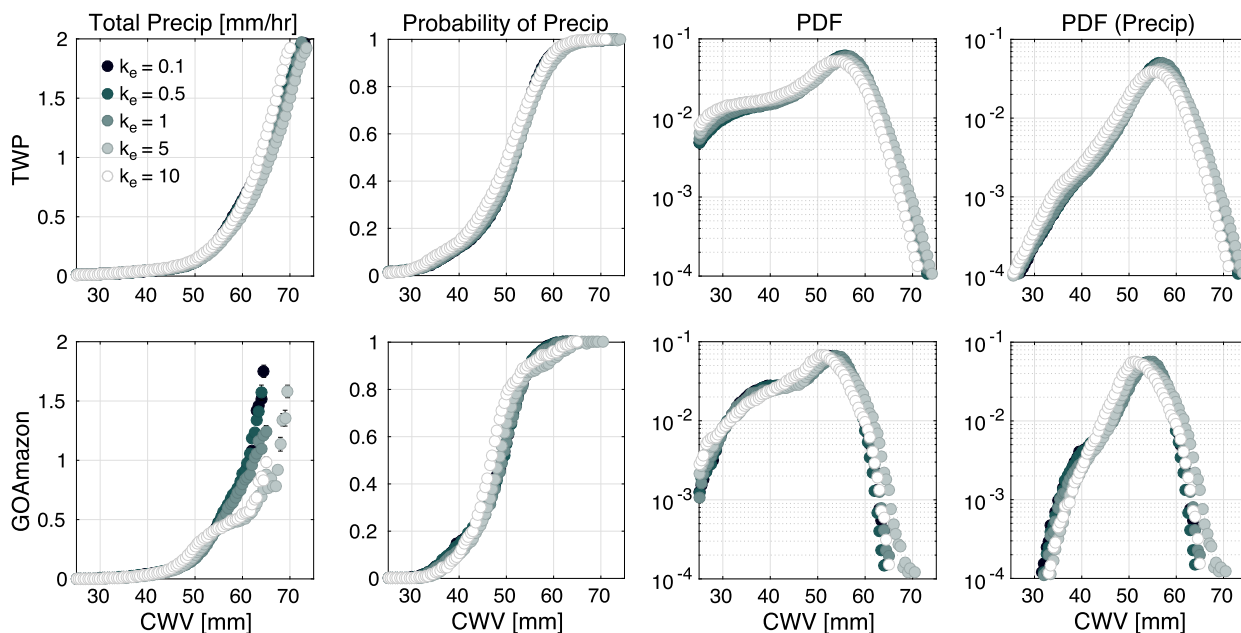


FIG. 6. The CESM-simulated convective transition statistics (top) in the tropical western Pacific and (bottom) at the GOAmazon site for various reevaporation (k_e) cases. (left)–(right) The total precipitation rate conditioned on CWV, conditional probability of precipitation ($P > 0.1 \text{ mm h}^{-1}$), and PDFs of CWV for all and precipitating ($P > 0.1 \text{ mm h}^{-1}$) events. The standard errors associated with total precipitation rate are plotted if greater than that represented by the marker size. Underpopulated bins ($\text{PDF} < 10^{-4}$) are trimmed.

suggesting a shift from the deep convection regime to the large-scale saturation regime as the CWV is driven to large-scale saturation.

It is clear that the model can reproduce the pickup only with substantial entrainment. These convective transition statistics are drastically altered as dmpdz increases from 0 to 0.08. Further increase in dmpdz above 0.16 causes relatively minor changes in the pickup behavior. These results apply for both maritime and continental tropics. The dependences of climatological values on entrainment we see in Fig. 2, together with the convective transition statistics shown in Figs. 4 and 5, clearly demonstrate the dominant direction in the fast-time-scale precipitation–CWV relationship, indicating that entrainment results in the observed precipitation pickup, and the importance of environmental humidity to convective onset, in line with previous studies.

6. Effects of varying precipitation reevaporation

Reevaporation of precipitation could be hypothesized to affect the relationship between precipitation and CWV but via a different mechanism (i.e., greater reevaporation of hydrometeors in a drier environment reducing surface precipitation). Kim et al. (2011, their Fig. 12) found an impact of reevaporation on pickup at daily time scale, in terms of CRH, in an earlier version of

CAM (i.e., the precipitation picks up at lower CRH when subject to lower reevaporation rate). To evaluate the importance of this at the fast time scales most relevant to convection, we examine another set of CESM cases with varying reevaporation rate k_e . In the CAM, reevaporation is modeled following Sundqvist (1988), where the evaporation rate of convective precipitation is proportional to $1 - \text{RH}$ and a prescribed value of k_e . Here RH is the relative humidity at each level.

The simulated climatologies in the tropics are insensitive to reevaporation, except that the temperature decreases by about 1.5 K across the large range examined, and the precipitation rates over land decrease modestly, in response to increasing k_e (see Fig. B1). The corresponding convective transition statistics for the whole tropical western Pacific basin (TWP; west to 170°W) and for the GOAmazon site are compiled in Fig. 6. Much like the climatological responses, the precipitation pickup and the associated statistics (including convective precipitation; not shown) are insensitive to k_e across the two orders of magnitude tested here (from 0.1 to 10), except for large k_e values (5 and 10) for GOAmazon, where a slight reduction in the highest conditional average rain rates at high CWV may be noted. Though not the main focus here, the sensitivity noted in Kim et al. (2011) may be attributed to changing temperature in response to varying reevaporation (see Figs. B1 and B2).

Overall, the insensitivity to reevaporation shown in Fig. 6 suggests that reevaporation cannot be the primary cause for the precipitation pickup.

7. Temporal relation between CWV and precipitation revisited

Figure 7 shows the same composites as in Fig. 1, but for the no-entrainment case. In this case, one does not see an increase in CWV or CRH associated with the occurrence of high precipitation. At Manus Island, there is essentially no change in CWV, CRH, or \widehat{q}_{sat} when composited on precipitation. At the GOAmazon site for the no-entrainment case, the diurnal cycle overwhelmingly predominates the variations in precipitation as well as in CWV, CRH, and \widehat{q}_{sat} . Without dependence on lower-tropospheric environmental humidity set by entrainment, the influence of the diurnal cycle seems to be exaggerated. Diurnal cycle aside, composites for both tropical maritime and continental locations are consistent with the convective transition statistics (Figs. 4 and 5), showing that the precipitation and environmental humidity are no longer closely related when entrainment is turned off, and both the environmental humidity and temperature fail to serve as an indicator for precipitation.

8. Discussion

This study analyzes simulations from a set of parameter perturbation experiments in coupled CESM1 to determine the dominant direction of causality in the fast-time-scale precipitation–water vapor relationship. The results presented here include composite time series centered at locally high precipitation (Figs. 1 and 7), the climatological responses at the largest tropical scales to varying entrainment (Figs. 2 and 3), and the dependences of the set of statistics associated with the transition to deep convection (referred to as convective transition statistics; Figs. 4–6) on entrainment and reevaporation. The simulated convective transition statistics, in comparison to ground-based observations from ARM sites in the tropical western Pacific and from the GOAmazon campaign, as well as satellite microwave retrievals over tropical ocean basins lead us to conclude that entrainment results in the observed pickup of precipitation with CWV. This conclusion is in line with previous studies including the conditional instability calculations for entraining plumes. Unlike the offline entraining plume calculations, the CESM takes into account the two-way interaction between deep convection and environmental humidity, including moistening of the environment through detrainment

and parameterized reevaporation of hydrometeors. When substantial entrainment is included in the deep convective parameterization, the composite time series (Fig. 1) show that the CWV increases prior to and decreases after (convective) precipitation maximum, akin to the observed (Fig. A1; Holloway and Neelin 2010) association with precipitation.

The high CWV associated with convection in these time series, and in the convective transition statistics, has been hypothesized to be due to the impacts of environmental humidity on deep convection through entrainment in the lower free troposphere. The devil's advocate position, on the other hand, would be to postulate that these associations are simply due to the effect of convective moistening via detrainment or reevaporation. There is not sufficient asymmetry in the lead–lag relationship to rule out convective moistening as a major pathway. However, these parameter perturbation experiments add a new line of evidence for the causal role of entrainment. With low values of entrainment in the deep convective scheme (shallow convection is not affected), the convective transition statistics show a breakdown of the precipitation pickup, and the composite time series of CWV and precipitation are no longer tied together. Convection in this case occurs without preconditioning of environmental humidity, resulting in a dry and relatively warm atmosphere. In contrast, with substantial entrainment, the high CWV associated with convection in the corresponding composite time series and convective transition statistics indicate that convection cannot fire until the lower-free-tropospheric environment is moistened as a result of the impact on buoyancy of turbulent entrainment of dry versus moist air, resulting in a moist and relatively cool atmosphere. The pathway through reevaporation is likely inconsequential to the existence of the pickup since varying the reevaporation rate by two orders of magnitude results in only minor variations in the convective transition statistics, although it can quantitatively affect the climatology (Fig. B1).

As far as the precipitation–CWV relationship and its dependence on entrainment and reevaporation is concerned, the convective transition statistics at tropical maritime and continental sites are qualitatively very similar, though the convective transition statistics are more sensitive to reevaporation over land, where the influence of the diurnal cycle at low entrainment is also more significant.

Describing the convective transition statistics in terms of column-integrated values is primarily motivated by the availability of observational CWV products, including the ground-based radiometer data analyzed in the coordinated observational paper (Schiro et al. 2016).

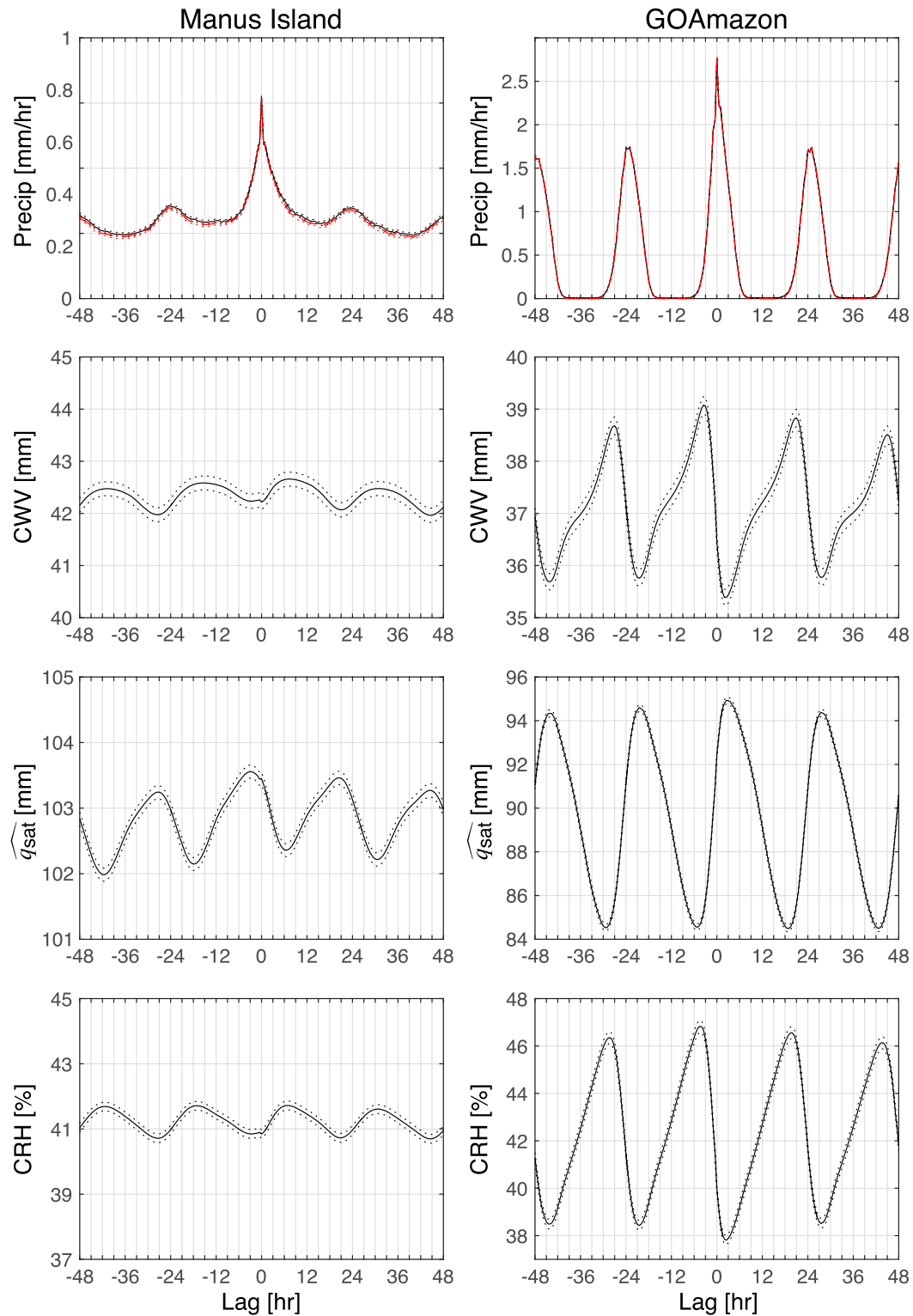


FIG. 7. As in Fig. 1, but for the no-entrainment case ($dmpdz = 0$). Note that the scales of the ordinates for plots at the GOAmazon site are different from those at Manus Island or those shown in Fig. 1. At both sites, one can hardly differentiate total and convective precipitation, owing to the lack of large-scale precipitation, and the composites centered at locally high convective and total precipitation are quantitatively similar in this case.

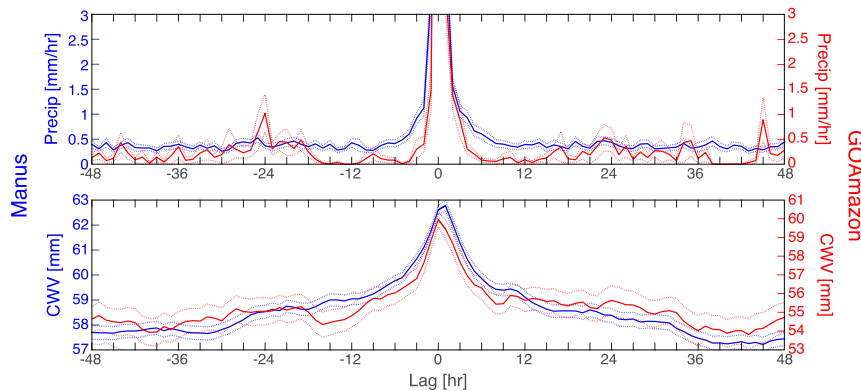


FIG. A1. Composite time series for CWV and precipitation rate centered at locally high (total) precipitation rate calculated using radiometer and rain gauge data (hourly mean) collected for the period 1998–2010 at Manus Island (blue) and for the period 10 Jan 2014–20 Oct 2015 at the GOAmazon site (red). The qualitative features indicated by these curves are robust with respect to the threshold defining heavy precipitation. The maximum of precipitation composites is about 19 mm h^{-1} at Manus and about 18 mm h^{-1} at the GOAmazon site.

It retains information of environmental impacts on conditional instability of the deepest vertical structures of moisture variations, although not of more detailed vertical structure variations. Quantitative differences in the precipitation pickup (e.g., critical CWV and \widehat{q}_{sat} ; not shown) are observed across different ocean basins and may be attributed to this. One way to quantify the uncertainties of convective transition statistics due to vertical structure is to treat these hidden factors as stochastic processes (e.g., Neelin et al. 2009), but ideally additional information about vertical structure should be included (i.e., explicitly distinguishing between boundary layer and lower-free-troposphere impacts on conditional instability). Convective transition statistics in GCMs (Sahany et al. 2012, 2014) require high-time-resolution output or instantaneous samples of variables important for convection, which are not yet standard output in most models.

The results here are obtained with a single coupled GCM (CESM) that uses a particular convective parameterization. In this regard, our findings are model dependent. Nevertheless, our focus has been a specific process that is represented in a qualitatively similar way in other current convective parameterizations. Differences among various convective parameterizations include the vertical profile of entrainment rate. Other studies have analyzed simulations subject to different entrainment characteristics and have concluded that the entrainment profile can impact large-scale features such as double-ITCZ bias (e.g., Hirota et al. 2014). The present study finds that the impacts of entrainment on the climatological simulation at the largest tropical scales, while substantial, are not as dramatic as those

seen at the fast time scales analyzed here. This suggests that convective transition statistics can provide additional diagnostics of model performance, addressing behavior at time scales closer to the parameterized process. Examination of these fast-process statistics in perturbed physics experiments helps to determine which aspects of the underlying physics are being constrained by these metrics. This provides essential background as convective-transition statistics are used to calibrate GCMs. Quantitative comparisons require quantification of dependence on temporal and spatial resolutions as well as differences among reanalysis/satellite retrieval and ground-based observational products. However, qualitative conclusions such as the complete collapse of major features of the observations for low entrainment noted here are expected to be robust. More importantly, the model-based results can answer questions that cannot be addressed with observations alone, such as the relative importance of a particular physical process.

Acknowledgments. This research was supported by the Office of Biological and Environmental Research of the U.S. Department of Energy Grant DE-SC0011074, National Oceanic and Atmospheric Administration Grants NA14OAR4310274 and NA15OAR4310097, and National Science Foundation Grant AGS-1540518. U.S. Department of Energy Atmospheric Radiation Measurement (ARM) Climate Research Facility GOAmazon and tropical western Pacific field campaign data are acknowledged. We thank K. Schiro for discussions in coordinating with her observational analysis, and for assistance with ARM site data, and J. Meyerson for graphical assistance. We also thank an anonymous

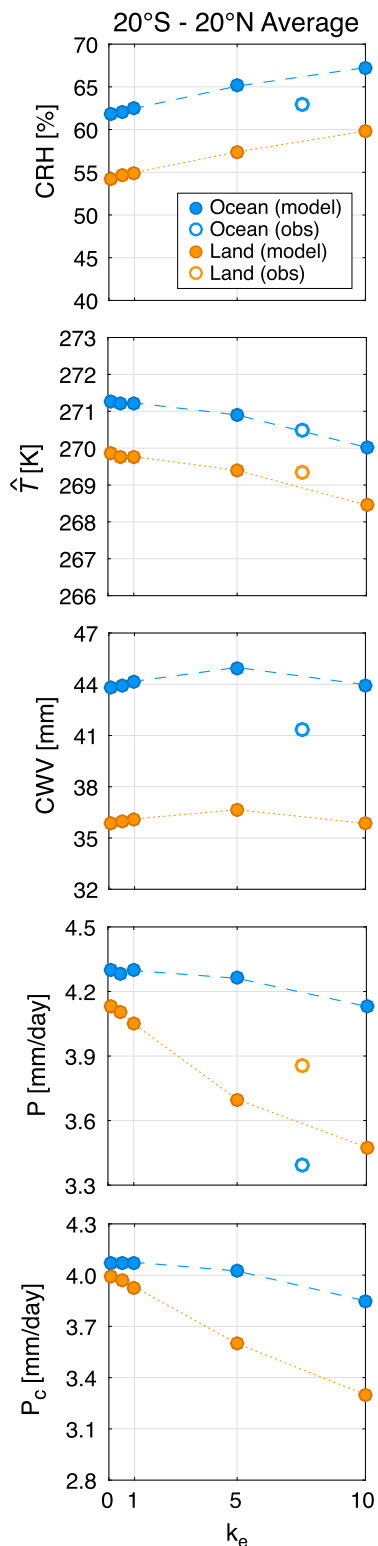


FIG. B1. As in Fig. 2, but for $k_e = 0.1, 0.5, 1, 5,$ and 10 .

reviewer for suggesting the addition of the reevaporation sensitivity experiments. A portion of this work has previously been presented at an American Geophysical Union meeting (Neelin et al. 2015).

APPENDIX A

Lead-Lag Relationship between CWV and Precipitation

Figure A1 shows the composites centered at locally high total precipitation calculated using the radiometer and rain gauge data (hourly mean) collected from the ARM site for the period of 1998–2010 at Manus Island and for the period from 10 January 2014 through 20 October 2015 during the GOAmazon campaign. Here high precipitation is defined as being greater than the mean precipitation rate averaged over all precipitating events with respect to the threshold value of 0.1 mm h^{-1} .

At both locations, CWV gradually increases (decreases) before (after) the precipitation peaks, with more drastic variation occurs between $\pm 6\text{-h}$ time lag, which could be attributed to mesoscale processes. It is clear that CWV has a longer autocorrelation time scale compared with precipitation. At the GOAmazon site, there are secondary precipitation peaks 24 h before and after the main peak, hinting to the diurnal cycle. At Manus Island, the CWV slightly lags the precipitation maximum by about 7 min (from the original higher-time-resolution data; not shown), and the precipitation rate outside the main peak is invariant in time. Overall, the composites are rather symmetric.

The composites from the standard-entrainment case (see Figs. 1 and S1) qualitatively capture the relationship between environmental humidity and precipitation seen from observations, although quantitative differences do exist. For instance, the simulated precipitation as well as the CWV variation associated with strong precipitation is smaller than in observations and have a longer time scale of increase prior and decrease after. The amplitudes of the simulated diurnal cycle are probably exaggerated. These discrepancies may due partly to the model resolution.

It is also worth noting that calculations of the simulated precipitation diurnal cycle using the 30-yr-long history at the geographical location of the GOAmazon site exhibit numerical wiggles at 1-h period (two half-hour steps). These wiggles are not large enough to affect conclusions here but serve as a reminder that examining models for convective time-scale processes can reveal imperfections in model numerics and implications for the fundamental underlying physics.

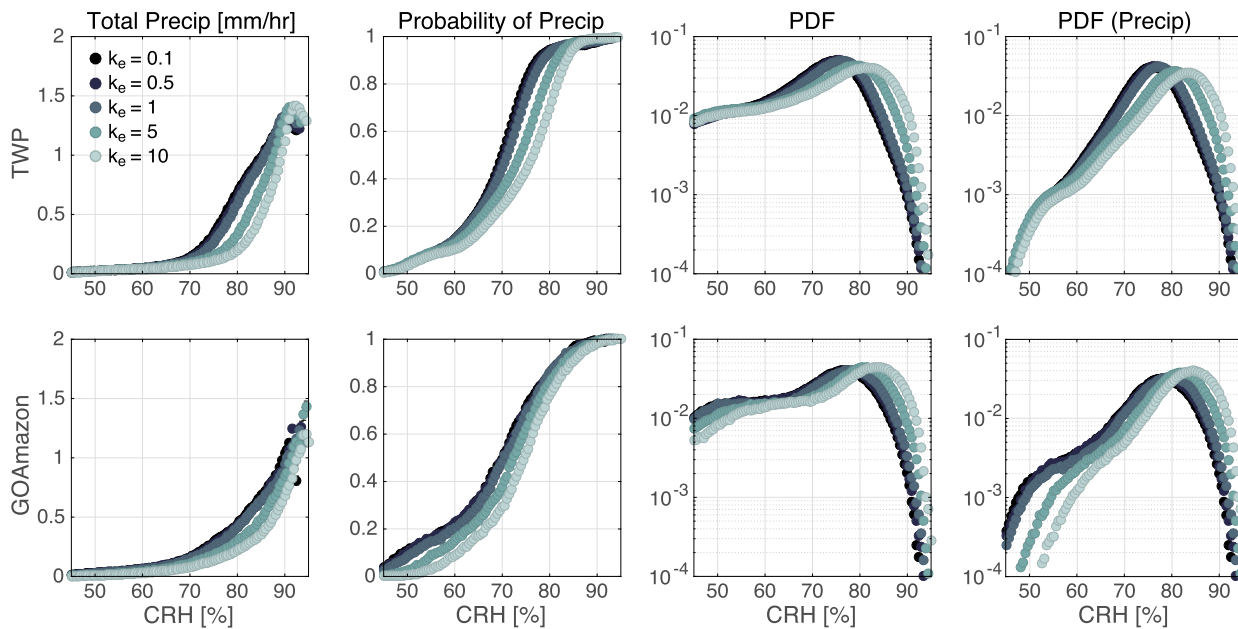


FIG. B2. As in Fig. 6, but for CRH.

APPENDIX B

Climatological Responses to Varying Reevaporation

Figure B1 shows the simulated climatologies averaged over the tropics as a function of reevaporation rate k_e . As in Fig. 2, values for ocean and land points are calculated separately, and the corresponding values from observations/reanalysis are also provided for reference. Overall, the climatological responses to varying k_e across the range examined here are smaller compared with those for dmpdz as in Fig. 2. The average \bar{T} drops by about 1.5 K as k_e increases from 0.1 to 10, while CWV changes about 1 mm. At the same time, the average CRH increases by about 5%, associated with the changing temperature. Both the total and convective precipitation rates are insensitive to increasing k_e over ocean but decrease modestly over land. The ratio of convective to total precipitation is almost constant ($74\% \pm 1\%$), with slight reduction for $k_e = 10$ (71% over ocean vs 69% over land). Thus k_e does have nontrivial impacts on the climatology, especially over land.

The simulated fast-time-scale statistics for various k_e values are compiled again in Fig. B2, but with CWV replaced by CRH. These statistics show modest sensitivity to reevaporation, but given the results in Figs. 6 and B1, this sensitivity is likely due to the change in temperature. We have not broken out the convective transition statistics with conditional averages on temperature, but previous results for observations and

related versions of CESM (Sahany et al. 2014) show that convective onset is not well approximated by constant CRH—as \widehat{q}_{sat} increases, the onset occurs at lower values of CRH. Thus the modest differences in Fig. B2 relative to Fig. 6 are likely an artifact of using CRH versus CWV to characterize the impact of environmental humidity on conditional instability.

REFERENCES

- Adams, D. K., S. I. Gutman, K. L. Holub, and D. S. Pereira, 2013: GNSS observations of deep convective time scales in the Amazon. *Geophys. Res. Lett.*, **40**, 2818–2823, doi:10.1002/grl.50573.
- Adler, R., and Coauthors, 2003: The Version-2 Global Precipitation Climatology Project (GPCP) monthly precipitation analysis (1979–present). *J. Hydrometeorol.*, **4**, 1147–1167, doi:10.1175/1525-7541(2003)004<1147:TVGPCP>2.0.CO;2.
- Bechtold, P., J. Chaboureaud, A. Beljaars, A. K. Betts, M. Kohler, M. J. Miller, and J. Redelsperger, 2004: The simulation of the diurnal cycle of convective precipitation over land in a global model. *Quart. J. Roy. Meteor. Soc.*, **130**, 3119–3137, doi:10.1256/qj.03.103.
- , M. Kohler, T. Jung, F. Doblas-Reyes, M. Leutbecher, M. J. Rodwell, F. Vitart, and G. Balsamo, 2008: Advances in simulating atmospheric variability with the ECMWF model: From synoptic to decadal time-scales. *Quart. J. Roy. Meteor. Soc.*, **134**, 1337–1351, doi:10.1002/qj.289.
- Benedict, J. J., E. D. Maloney, A. H. Sobel, and D. M. W. Frierson, 2014: Gross moist stability and MJO simulation skill in three full-physics GCMs. *J. Atmos. Sci.*, **71**, 3327–3349, doi:10.1175/JAS-D-13-0240.1.
- Bernstein, D. N., and J. D. Neelin, 2016: Identifying sensitive ranges in global warming precipitation change dependence on convective parameters. *Geophys. Res. Lett.*, **43**, 5841–5850, doi:10.1002/2016GL069022.

- Bretherton, C. S., M. E. Peters, and L. E. Back, 2004: Relationships between water vapor path and precipitation over the tropical oceans. *J. Climate*, **17**, 1517–1528, doi:10.1175/1520-0442(2004)017<1517:RBWVPA>2.0.CO;2.
- Brown, R. G., and C. Zhang, 1997: Variability of midtropospheric moisture and its effect on cloud-top height distribution during TOGA COARE. *J. Atmos. Sci.*, **54**, 2760–2774, doi:10.1175/1520-0469(1997)054<2760:VOMMAI>2.0.CO;2.
- Del Genio, A. D., and J. Wu, 2010: The role of entrainment in the diurnal cycle of continental convection. *J. Climate*, **23**, 2722–2738, doi:10.1175/2009JCLI3340.1.
- , Y. Chen, D. Kim, and M.-S. Yao, 2012: The MJO transition from shallow to deep convection in *CloudSat*/CALIPSO and GISS GCM simulations. *J. Climate*, **25**, 3755–3770, doi:10.1175/JCLI-D-11-00384.1.
- Derbyshire, S. H., I. Beau, P. Bechtold, J.-Y. Gandpeix, J.-M. Piriou, J.-L. Redelsperger, and P. Soares, 2004: Sensitivity of moist convection to environmental humidity. *Quart. J. Roy. Meteor. Soc.*, **130**, 3055–3079, doi:10.1256/qj.03.130.
- Gent, P. R., and Coauthors, 2011: The Community Climate System Model version 4. *J. Climate*, **24**, 4973–4991, doi:10.1175/2011JCLI4083.1.
- Hannah, W. M., and E. D. Maloney, 2014: The moist static energy budget in NCAR CAM5 hindcasts during DYNAMO. *J. Adv. Model. Earth Syst.*, **6**, 420–440, doi:10.1002/2013MS000272.
- Hilburn, K. A., and F. J. Wentz, 2008: Intercalibrated passive microwave rain products from the Unified Microwave Ocean Retrieval Algorithm (UMORA). *J. Appl. Meteor. Climatol.*, **47**, 778–794, doi:10.1175/2007JAMC1635.1.
- Hirota, H., Y. N. Takayabu, M. Watanabe, M. Kimoto, and M. Chikira, 2014: Role of convective entrainment in spatial distributions of and temporal variations in precipitation over tropical oceans. *J. Climate*, **27**, 8707–8723, doi:10.1175/JCLI-D-13-00701.1.
- Holloway, C. E., and J. D. Neelin, 2009: Moisture vertical structure, column water vapor, and tropical deep convection. *J. Atmos. Sci.*, **66**, 1665–1683, doi:10.1175/2008JAS2806.1.
- , and —, 2010: Temporal relations of column water vapor and tropical precipitation. *J. Atmos. Sci.*, **67**, 1091–1105, doi:10.1175/2009JAS3284.1.
- Hourdin, F., and Coauthors, 2013: LMDZ5B: The atmospheric component of the IPSL climate model with revisited parameterizations for clouds and convection. *Climate Dyn.*, **40**, 2193–2222, doi:10.1007/s00382-012-1343-y.
- Hurrell, J. W., and Coauthors, 2013: The Community Earth System Model: A framework for collaborative research. *Bull. Amer. Meteor. Soc.*, **94**, 1339–1360, doi:10.1175/BAMS-D-12-00121.1.
- Jensen, M. P., and A. D. Del Genio, 2006: Factors limiting convective cloud-top height at the ARM Nauru Island climate research facility. *J. Climate*, **19**, 2105–2117, doi:10.1175/JCLI3722.1.
- Kahan, W., 1965: Further remarks on reducing truncation errors. *Commun. ACM*, **8**, 40, doi:10.1145/363707.363723.
- Kanamitsu, M., W. Ebisuzaki, J. Woollen, S. Yang, J. Hnilo, M. Fiorino, and G. Potter, 2002: NCEP–DOE AMIP-II Reanalysis (R-2). *Bull. Amer. Meteor. Soc.*, **83**, 1631–1643, doi:10.1175/BAMS-83-11-1631.
- Khairoutdinov, M., and D. Randall, 2006: High-resolution simulation of shallow-to-deep convection transition over land. *J. Atmos. Sci.*, **63**, 3421–3436, doi:10.1175/JAS3810.1.
- Kim, D., A. H. Sobel, E. D. Maloney, D. M. W. Frierson, and I.-S. Kang, 2011: A systematic relationship between intraseasonal variability and mean state bias in AGCM simulations. *J. Climate*, **24**, 5506–5520, doi:10.1175/2011JCLI4177.1.
- Klingaman, N. P., and Coauthors, 2015a: Vertical structure and physical processes of the Madden-Julian oscillation: Linking hindcast fidelity to simulated diabatic heating and moistening. *J. Geophys. Res. Atmos.*, **120**, 4690–4717, doi:10.1002/2014JD022374.
- , X. Jiang, P. K. Xavier, J. Petch, D. Waliser, and S. J. Woolnough, 2015b: Vertical structure and physical processes of the Madden-Julian oscillation: Synthesis and summary. *J. Geophys. Res. Atmos.*, **120**, 4671–4689, doi:10.1002/2015JD023196.
- Kuang, Z., and C. S. Bretherton, 2006: A mass-flux scheme view of a high-resolution simulation of a transition from shallow to deep convection. *J. Atmos. Sci.*, **63**, 1895–1909, doi:10.1175/JAS3723.1.
- Langenbrunner, B., 2015: Quantifying uncertainty in precipitation climatology, twenty-first century change, and teleconnections in global climate models. Ph.D. dissertation, University of California, Los Angeles, ProQuest/UMI Publ. AAT 3738088, 125 pp.
- Lin, J.-L., 2007: The double-ITCZ problem in IPCC AR4 coupled GCMs: Ocean–atmosphere feedback analysis. *J. Climate*, **20**, 4497–4525, doi:10.1175/JCLI4272.1.
- Lintner, B. R., C. E. Holloway, and J. D. Neelin, 2011: Column water vapor statistics and their relationship to deep convection, vertical and horizontal circulation, and moisture structure at Nauru. *J. Climate*, **24**, 5454–5466, doi:10.1175/JCLI-D-10-05015.1.
- Madden, R. A., and P. R. Julian, 1971: Detection of a 40–50 day oscillation in the zonal wind in the tropical Pacific. *J. Atmos. Sci.*, **28**, 702–708, doi:10.1175/1520-0469(1971)028<0702:DOADOI>2.0.CO;2.
- Mapes, B. E., and R. B. Neale, 2011: Parameterizing convective organization to escape the entrainment dilemma. *J. Adv. Model. Earth Syst.*, **3**, M06004, doi:10.1029/2011MS000042.
- Mather, J. H., T. P. Ackerman, W. E. Clements, F. J. Barnes, M. D. Ivey, L. D. Hatfield, and R. M. Reynolds, 1998: An atmospheric radiation and cloud station in the tropical western Pacific. *Bull. Amer. Meteor. Soc.*, **79**, 627–642, doi:10.1175/1520-0477(1998)079<0627:AARACS>2.0.CO;2.
- Mechoso, C. R., and Coauthors, 1995: The seasonal cycle over the tropical Pacific in coupled ocean–atmosphere general circulation models. *Mon. Wea. Rev.*, **123**, 2825–2838, doi:10.1175/1520-0493(1995)123<2825:TSCOTT>2.0.CO;2.
- Neale, R. B., and Coauthors, 2010: Description of the NCAR Community Atmosphere Model (CAM 4.0). NCAR Tech. Note NCAR/TN-485+STR, 224 pp. [Available online at http://www.cesm.ucar.edu/models/ccsm4.0/cam/docs/description/cam4_desc.pdf.]
- , J. H. Richter, and M. Jochum, 2008: The impact of convection on ENSO: From a delayed oscillator to a series of events. *J. Climate*, **21**, 5904–5924, doi:10.1175/2008JCLI2244.1.
- Neelin, J. D., O. Peters, and K. Hales, 2009: The transition to strong convection. *J. Atmos. Sci.*, **66**, 2367–2384, doi:10.1175/2009JAS2962.1.
- , Y.-H. Kuo, K. A. Schiro, B. Langenbrunner, C. R. Mechoso, S. Sahany, and D. N. Bernstein, 2015: Tropical convective onset statistics and establishing causality in the water vapor–precipitation relation. *2015 Fall Meeting*, San Francisco, CA, Amer. Geophys. Union, Abstract A531-01.
- Oueslati, B., and G. Bellon, 2013: Convective entrainment and large-scale organization of tropical precipitation: Sensitivity of the CNRM-CM5 hierarchy of models. *J. Climate*, **26**, 2931–2946, doi:10.1175/JCLI-D-12-00314.1.

- , and —, 2015: The double ITCZ bias in CMIP5 models: Interaction between SST, large-scale circulation and precipitation. *Climate Dyn.*, **44**, 585–608, doi:10.1007/s00382-015-2468-6.
- Parsons, D. B., K. Yoneyama, and J.-L. Redelsperger, 2000: The evolution of the tropical western Pacific atmosphere-ocean system following the arrival of a dry intrusion. *Quart. J. Roy. Meteor. Soc.*, **126**, 517–548, doi:10.1002/qj.49712656307.
- Peters, O., and J. D. Neelin, 2006: Critical phenomena in atmospheric precipitation. *Nat. Phys.*, **2**, 393–396, doi:10.1038/nphys314.
- Raymond, D. J., and A. M. Blyth, 1986: A stochastic mixing model for nonprecipitating cumulus clouds. *J. Atmos. Sci.*, **43**, 2708–2718, doi:10.1175/1520-0469(1986)043<2708:ASMMFN>2.0.CO;2.
- Redelsperger, J.-L., D. B. Parsons, and F. Guichard, 2002: Recovery processes and factors limiting cloud-top height following the arrival of a dry intrusion observed during TOGA COARE. *J. Atmos. Sci.*, **59**, 2438–2457, doi:10.1175/1520-0469(2002)059<2438:RPAFLC>2.0.CO;2.
- Richter, J. H., and P. J. Rasch, 2008: Effects of convective momentum transport on the atmospheric circulation in the Community Atmosphere Model, version 3. *J. Climate*, **21**, 1487–1499, doi:10.1175/2007JCLI1789.1.
- Ridout, J., 2002: Sensitivity of tropical Pacific convection to dry layers at mid- to upper levels: Simulation and parameterization tests. *J. Atmos. Sci.*, **59**, 3362–3381, doi:10.1175/1520-0469(2002)059<3362:SOTPCT>2.0.CO;2.
- Rio, C., F. Hourdin, J.-Y. Grandpeix, and J.-P. Lafore, 2009: Shifting the diurnal cycle of parameterized deep convection over land. *Geophys. Res. Lett.*, **36**, L07809, doi:10.1029/2008GL036779.
- Romps, D. M., and Z. Kuang, 2010: Do undiluted convective plumes exist in the upper tropical troposphere? *J. Atmos. Sci.*, **67**, 468–484, doi:10.1175/2009JAS3184.1.
- Sahany, S., J. D. Neelin, K. Hales, and R. B. Neale, 2012: Temperature–moisture dependence of the deep convective transition as a constraint on entrainment in climate models. *J. Atmos. Sci.*, **69**, 1340–1358, doi:10.1175/JAS-D-11-0164.1.
- , —, —, and —, 2014: Deep convective transition characteristics in the NCAR CCSM and changes under global warming. *J. Climate*, **27**, 9214–9232, doi:10.1175/JCLI-D-13-00747.1.
- Sanderson, B. M., 2011: A multimodel study of parametric uncertainty in predictions of climate response to rising greenhouse gas concentrations. *J. Climate*, **24**, 1362–1377, doi:10.1175/2010JCLI3498.1.
- Shiro, K. A., J. D. Neelin, D. K. Adams, and B. R. Linter, 2016: Deep convection and column water vapor over tropical land versus tropical ocean: A comparison between the Amazon and the tropical western Pacific. *J. Atmos. Sci.*, **73**, 4043–4063, doi:10.1175/JAS-D-16-0119.1.
- Sherwood, S. C., and R. Wahrlich, 1999: Observed evolution of tropical deep convective events and their environment. *Mon. Wea. Rev.*, **127**, 1777–1795, doi:10.1175/1520-0493(1999)127<1777:OEOTDC>2.0.CO;2.
- , S. Bony, and J.-L. Dufresne, 2014: Spread in model climate sensitivity traced to atmospheric convective mixing. *Nature*, **505**, 37–42, doi:10.1038/nature12829.
- Smith, R. D., and Coauthors, 2010: The Parallel Ocean Program (POP) reference manual: Ocean component of the Community Earth System Model (CESM) and Community Earth System Model (CESM). Los Alamos National Laboratory Tech. Rep. LAUR-10-01853, 141 pp. [Available online at <http://www.cesm.ucar.edu/models/cesm1.0/pop2/doc/sci/POPRefManual.pdf>.]
- Sobel, A. H., S. E. Yuter, C. S. Bretherton, and G. N. Kiladis, 2004: Large-scale meteorology and deep convection during TRMM KWAJEX. *Mon. Wea. Rev.*, **132**, 422–444, doi:10.1175/1520-0493(2004)132<0422:LMADCD>2.0.CO;2.
- Stokes, G. M., and S. E. Schwartz, 1994: The Atmospheric Radiation Measurement (ARM) program: Programmatic design of the cloud and radiation test bed. *Bull. Amer. Meteor. Soc.*, **75**, 1201–1221, doi:10.1175/1520-0477(1994)075<1201:TARMPP>2.0.CO;2.
- Sundqvist, H., 1988: Parameterization of condensation and associated clouds in models for weather prediction and general circulation simulation. *Physically-Based Modeling and Simulations of Climate and Climate Change*, M. E. Schlesinger, Ed., Vol. 1, Kluwer Academic, 433–461.
- Tompkins, A. M., 2001: Organization of tropical convection in low vertical wind shears: The role of water vapor. *J. Atmos. Sci.*, **58**, 529–545, doi:10.1175/1520-0469(2001)058<0529:OOTCIL>2.0.CO;2.
- Waliser, D. E., B. Tian, X. Xie, W. T. Liu, M. J. Schwartz, and E. J. Fetzer, 2009: How well can satellite data characterize the water cycle of the Madden-Julian Oscillation? *Geophys. Res. Lett.*, **36**, L21803, doi:10.1029/2009GL040005.
- Zhang, G. J., and N. A. McFarlane, 1995: Sensitivity of climate simulations to the parameterization of cumulus convection in the Canadian Climate Centre general circulation model. *Atmos.–Ocean*, **33**, 407–446, doi:10.1080/07055900.1995.9649539.
- Zhu, H., and H. Hendon, 2015: Role of large-scale moisture advection for simulation of the MJO with increased entrainment. *Quart. J. Roy. Meteor. Soc.*, **141**, 2127–2136, doi:10.1002/qj.2510.